Contents list available at CBIORE journal website

International Journal of Renewable Energy Development

Journal homepage: https://ijred.cbiore.id

Research Article

Model free control of hybrid fuel-cell and supercapacitor powered electric vehicle

Tejas Narsing Dhanagare[a], Qiaohui He[b], Vedantham Lakshmi Srinivas[a], Abdoalateef Alzhrani[c*], A. S. Vardhan[d], Madhu Singh[d], R. K. Saket[e], Xiaowei Zhao[b]

[a] *Department of Electrical Engineering at Indian Institute of Technology (Indian School of Mines), Dhanbad, Jharkhand, 826004, India.*

[b] *Intelligent Control and Smart Energy Research Lab, School of Engineering, University of Warwick, Coventry CV4 7AL, United Kingdom.*

[c] *Department of Electrical Engineering, Jubail Industrial College, Jubail Industrial City, Saudi Arabia*

[d] *Department of Electrical Engineering, National Institute of Technology, Jamshedpur, Jharkhand, 831014, India.*

[e] *Department of Electrical Engineering at Indian Institute of Technology (Banaras Hindu University), Varanasi, Uttar Pradesh, 221005, India.*

Abstract. This paper proposes a novel model-free control (MFC) strategy for hybrid electric vehicles (EVs) powered by a proton exchange membrane fuel cell (PEMFC) and a supercapacitor (SC). Unlike conventional model-based approaches that depend on accurate system identification and parameter tuning, the proposed framework employs ultra-local models to adapt dynamically to system variations without explicit modeling. The hybrid architecture is implemented using an interleaved boost converter for the PEMFC and a bidirectional buck–boost converter for the SC, coordinated to supply propulsion power and enable regenerative braking. Comprehensive MATLAB/Simulink simulations demonstrate that the proposed MFC achieves <3% current tracking error for both PEMFC and SC, ~750 ms settling time for PMSM speed variations, and <120 ms response for power transitions, while the DC bus voltage remains tightly regulated under dynamic load disturbances. Hardware-in-the-loop (HIL) validation on an OPAL-RT 5600 platform further confirms the method's feasibility, showing a 20% reduction in execution time and enhanced robustness against parameter uncertainties compared to classical PI control. Experimental results also verify stable current sharing in interleaved converters, accurate voltage regulation in the SC branch, and smooth torque generation in the PMSM drive. Overall, the proposed control strategy provides a computationally efficient, fault-tolerant, and plug-and-play solution for next-generation EVs by reducing calibration effort and ensuring reliable operation under nonlinear and uncertain conditions, while demonstrating clear potential for real-time automotive applications.

Keywords: Fuel-cell, Hybrid electric vehicle, Energy storage, Power electronic control, Permanent magnet synchronous motor (PMSM) and Supercapacitor

Received: 2nd Feb 2025; Revised: 15th August 2025; Accepted: 28th Oct 2025; Available online: 30th Dec 2025

1. Introduction

The rapid depletion of oil and natural gas resources, as well as the concerns of global warming and fossil fuel depletion, are pushing the development of alternative vehicle systems technology. As a result, a growing number of studies on fuel cell electric vehicles (EVs) have been done (Chanda *et al.* 2024). The fuel cell stack is typically used in conjunction with energy storage devices (ESS) due to the sluggish dynamic reaction and inability to soak up braking energy (Romli *et al.* 2016). The fuel cell will largely sustain the vehicle's typical load power, while the battery will let the fuel cell provide the peak power or absorb regenerative braking energy. Meanwhile, the supercapacitor handles the quickly changing high-frequency load power needs (Romli *et al.* 2016). The function of DC/DC converter control is to guarantee the dynamic energy interchange between the fuel-cell stack, ESS modules and the EV drive loads (Benayed *et al.* 2021 & Srinivas *et al.* 2020).

A DC-DC converter can be controlled in a variety of ways to balance the current or power flowing through each of its inductor cells, including the traditional proportional-integral (PI) control (Teng *et al* 2024), sliding mode control (Renaudineau *et al.* 2014 & G. Huang *et al.* 2022), and differential flatness control (Thounthong *et al.* 2010). When parameter variance is considered, the boost DC/DC converter model is uncertain, whereas the methods suggested in (Teng *et al* 2024 & Renaudineau *et al.* 2014 & Thounthong *et al.* 2010) are all model-based control concepts. While DC/DC converters are used for dynamic energy exchange between energy storage device and EV drive converters, the PMSMs are used for necessary torque production for EV drive. PMSMs are widely adopted for electric power drives in a variety of fields due to multiple advantages such as high power-weight ratio, low maintenance cost, and simple design, which has led to the development of a wholly electric vehicle (Lie *et al.* 2018). There is various control schemes reported as follows. Predictive control provides the quickest dynamic reaction (Yang *et al.* 2017). The disruption and ambiguity are successfully rejected by the disturbance-observer-based control (Shetty *et al.* 2024). Incompletely

* Corresponding author
Email: abdoalateef@gmail.com (A.Alzhrani)

https://doi.org/10.61435/ijred.2026.61095
ISSN: 2252-4940/© 2026.The Author(s). Published by CBIORE

described systems have been successfully controlled by the Takagi-Sugeno flexible model (Vu *et al.* 2013). Other control strategies for PMSMs include adaptive control (Kim *et al.* 2017), resilient control (Soricellis *et al.* 2018), and neural network control (El-Sousy *et al.* 2013). Recently, (Kommula *et al.* 2019, Ge 2024, Sriprang *et al.* 2019 & Srinivas *et al.* 2022) suggested the flatness-based control and expanded Luenberger observer for PMSM control. Although the controls of PMSMs have been described in these studies, factors such as their nonlinearity and parameter uncertainty make obtaining a control system with high performance challenging (Khan *et al.* 2019).

All the aforementioned DC/DC converter controllers and PMSM drive controls are system model-based, where the controllers necessitate the system model parameters. To overcome the drawbacks in model-based controllers, some researchers have proposed model-free control (MFC) technique (Mustafa *et al.* 2019) because, when compared to the model-based control method, it lessens reliance on model information. The fundamental principle of MFC management is to split the overall system model into an ultra-local model with the system's input and output (Mustafa *et al.* 2019 & Fliess *et al.* 2013). In (Mungporn *et al.* 2019), to manage the fuel-cell power for microgrid uses, a model-free control (MFC) theory based on the ultra-local model is investigated. The model-free control, which does not necessitate the employment of a decoupling approach for a permanent magnet synchronous generator, is presented by Sriprang *et al.* (Sriprang *et al.* 2019). To address key factors such as weighting factor and parameter mismatch, a model-free hybrid parallel predictive speed control (MF-HPPSC) based on an ultra-local model is suggested in (Gao *et al.* 2022). In all these model-free controls, it is observed that it has the benefit of not requiring all the system's parameters, unlike the model-based controls.

However, although model-free controls are contemplated with respect to converter controls in microgrid systems, the behavior of such control has not yet been investigated in hybrid energy storage powered electric vehicles. The model-based controls for hybrid energy storage powered EVs, are reported by (Vu *et al.* 2013), where the model parametric variations are observed to significantly affect the EV drive performance. To overcome the drawbacks of the model-based controller, this article suggests model-free control, wherein the EV propulsion system, including the fuel cell and supercapacitor, is made independent of the system parameters. Specifically, the PMSM based EV drive train is considered herein, with fuel cell (FC) and supercapacitor (SC) as energy storage and dispatch devices, owing to their high energy and power densities respectively, the primary power source being FC. To facilitate dynamic energy exchange between hybrid energy storages, EV drive trains and propulsion systems, various power converters are employed.

Building on the above, this study makes key contributions that advance the field. Hybrid electric vehicles (EVs) powered by proton exchange membrane fuel cells (PEMFC) and supercapacitors (SC) require effective control strategies to manage both propulsion and energy sources. This paper presents a model-free control (MFC) strategy that develops propulsion and energy management controls without relying on system modeling parameters. The proposed approach offers strong robustness to parametric variations, ensuring consistent performance and enhanced system reliability across a wide range of dynamic operating conditions. By eliminating the need for detailed mathematical models of the fuel cell, supercapacitor, and motor drive, this technique reduces design complexity and improves adaptability in real-time applications (Fliess and Join 2013; Benbouzid 2000).

Traditional model-based control approaches dominate current EV control systems, typically relying on accurate system identification, parameter estimation, and the design of complex observers or estimators (Emadi et al. 2008; Khaligh and Li 2010). While effective in controlled environments, these methods are highly sensitive to modeling inaccuracies, parameter drift caused by aging, thermal fluctuations, and manufacturing variability. Moreover, they require extensive offline calibration and are prone to performance degradation in the presence of unmodeled system dynamics or external disturbances (Wu et al. 2003; Li *et al.* 2017). These limitations create significant challenges for practical deployment in the diverse and nonlinear operational conditions encountered in EVs.

The proposed MFC framework directly addresses these challenges by utilizing ultra-local models based on real-time input-output data, allowing the control strategy to adapt dynamically to system changes without prior knowledge of internal system dynamics (Join and Fliess 2017). This eliminates the need for manual parameter tuning and significantly simplifies controller design. Additionally, the approach demonstrates inherent robustness against system nonlinearities, load disturbances, and time-varying behaviors, enabling plug-and-play capability across different vehicle platforms and hardware configurations (Wada and Shibata 2019; Li et al. 2018). Such adaptability is crucial for next-generation EVs that must operate reliably under uncertain or degraded conditions. Extensive simulations validate the accurate current tracking of both the fuel cell and supercapacitor, along with tight regulation of the DC bus voltage under various operating scenarios (Saad *et al.* 2021). Real-time hardware-in-the-loop (HIL) testing conducted on the OPAL-RT 5600 platform further confirms the feasibility of embedded implementation and real-world applicability. The control strategy effectively manages both power delivery and regenerative braking without compromising performance, highlighting its practical viability (Sun and Zhu 2020).

To the best of the authors' knowledge, a fully model-independent control framework for hybrid PEMFC–SC powered EV systems, supported by both simulation and real-time experimental validation, has not been previously reported. This gap in the literature underscores the significance of the proposed method, which provides a computationally efficient, fault-tolerant alternative to conventional model-based strategies. The approach is particularly suited for EV applications operating in uncertain, nonlinear, or harsh environments where traditional control methods often fail to maintain reliable performance (Zhang and Li 2022; Li and Chen 2019).

This research aims to develop and validate a model-free control strategy for a hybrid PEMFC–supercapacitor electric vehicle system that ensures robust, adaptive propulsion and energy management without requiring detailed system models or parameter tuning. The approach focuses on precise current tracking, DC bus voltage regulation, and efficient power coordination between energy sources under varying dynamic conditions. It seeks to enhance fault tolerance and simplify controller design while demonstrating real-time feasibility through simulations and hardware-in-the-loop testing, ultimately providing a scalable and computationally efficient solution for complex, nonlinear EV environments.

The remainder of the paper is organized as follows: Section II introduces the system architecture and the proposed methodology for model-free control design. Section III presents detailed simulation results and experimental results along with the discussions Finally, Section IV concludes the paper.

2. Methodology

The hybrid PEMFC (proton exchange membrane-based fuel cell) and SC powered PMSM based electric vehicle drive system

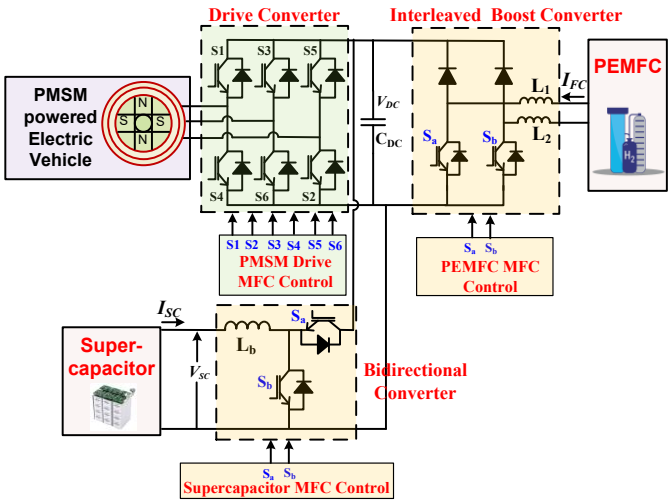

Fig. 1 Hybrid PEMFC-supercapacitor powered PMSM system schematic

are shown in Fig. 1. A 3-leg voltage source inverter is used to control the PMSM drive. It should be noted that an interleaved boost converter is implemented to the PEMFC instead of a normal boost converter since it can reduce the harmonics in the fuel cell current, which can extend the lifespan of the fuel cell (Hicham *et al.* 2021). A bidirectional buck-boost converter plays the role of power flow control for a supercapacitor (SC) since the SC not only outputs the power but also absorbs the energy. The model-free control strategies for each of the converters are derived in this section. Initially, the preliminaries of the model-free control are discussed. Later, the model-free control of PMSM, PEMFC and the supercapacitor are discussed in individual subsections.

2.1. Preliminaries of Model-Free Control

Fliess *et al.* established the concept of model-free control for control system applications. A general state-variable expression for a nonlinear system is represented as, $\dot{x} = f(x,u)$; $y = h(x,u)$, where x represents the state variable, u represents the input (control) variable, y represents the output variable (or measured variable) (Fliess *et al.* 2013) . An ultra-local model replaces the unknown "complex" mathematical model. This eliminates the need for precise mathematical modeling of the fuel cell, supercapacitor, and motor subsystems. The rationale for adopting the ultra-local model lies in its ability to represent the unknown and nonlinear dynamics of a physical system through a simplified input-output relationship of the form: (Fliess *et al.* 2013),

$$\dot{y} = -D + b \cdot u \tag{1}$$

where $\frac{\dot{y}}{b}$ is the system's only known component, and 'D' reflects all the other system dynamics. The block diagram of the control law for model-free based control is shown in Fig. 2. The controller law is defined as (Fliess *et al.* 2013),

$$u = u_{ref} + u_{feedback}(\varepsilon) + \hat{D}/b \tag{2}$$

where, $\hat{D}$ is the estimation of a defined unknown term, u_{ref} is reference term or known term $\varepsilon = y_{ref} - y_{measured}$, y_{ref} is the reference signal, and $y_{measured}$ is the measured signal. The control signals are:

$$u_{ref} = \dot{y}_{ref}/b \tag{3}$$

$$\hat{D} = b \cdot u - \dot{y} \tag{4}$$

substituting (2) in (1),

$$\dot{y} = -D + b \cdot u_{ref} + b \cdot u_{feedback}(\varepsilon) + \hat{D} \tag{5}$$

The estimation term seeks to offer an estimated value '$\hat{D}$' so that '$\hat{D}$' converges to 'D' is expressed as t→∞. The convergence of the MFC system is inherently guaranteed under the assumption that the estimation of D is sufficiently accurate over the control horizon. In practice, D is approximated using a finite difference-based estimator or real-time filters with negligible latency, enabling rapid feedback correction. The closed-loop system resembles a first-order linear system with guaranteed exponential tracking under nominal conditions. As a result, (5) can be expressed as,

$$\dot{y} = b \cdot u_{ref} + b \cdot u_{feedback}(\varepsilon) \tag{6}$$

As a result, provided the controller settings are specified correctly, equation (6) will converge to zero. As a result, setting (6) equivalent to zero produces,

$$b \cdot u_{ref} + b \cdot u_{feedback}(\varepsilon) = 0 \tag{7}$$

2.2. Model-Free control of PMSM

The non-salient PMSM basic rotating reference frame equations are shown as follows (Romli *et al.* 2016, Benayed *et al.* 2021, Srinivas *et al.* 2020 & Teng *et al.* 2024):

$$\begin{pmatrix} \dot{i_d} \\ \dot{i_q} \end{pmatrix} = \frac{1}{L_s}\begin{pmatrix} -R_s & \omega_e \cdot L_s \\ -R_s & -\omega_e \cdot L_s \end{pmatrix}\begin{pmatrix} i_d \\ i_q \end{pmatrix} + \frac{1}{L_s}\begin{pmatrix} v_d \\ v_q \end{pmatrix} + \frac{1}{L_s}\begin{pmatrix} 0 \\ \psi_m \end{pmatrix} \tag{8}$$

$$\dot{\omega_m} = \frac{1}{J}.\left(T_e - T_L - B_f \cdot \omega_m\right) \tag{9}$$

where,

$$T_e = n_p \cdot \Psi_m \cdot i_q \tag{10}$$

$$\frac{\omega_e}{\omega_m} = n_p \tag{11}$$

In (8), 'v_d' and 'v_q' are the d-axis , q-axis voltages, i_d and i_q are the d-axis , q-axis stator currents, R_s and Ψ_m are the resistances and permanent magnet flux linkage, respectively; and ω_e, ω_m, n_p, T_e, T_L ,B_f , J are electrical angular frequency, mechanical angular frequency, number of pole pairs, electromagnetic torque, load torque, viscosity, and inertia, respectively. The PMSM modelling equations (8)-(9) can be written in the format of (1),

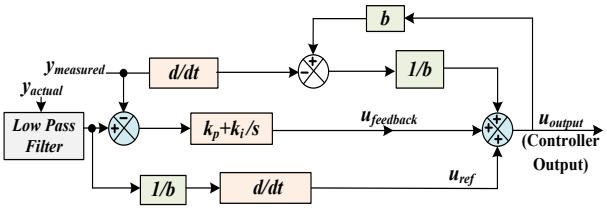

Fig. 2 Block diagram of the control law

by defining $u = [u_1\ u_2]^T = [v_d\ v_q]^T$ and $y = [y_1\ y_2]^T = [i_d\ i_q]^T$ as,

$$\dot{i_d} = -\frac{1}{L_s}.(R_s \cdot i_d - \omega_e \cdot L_s.i_q) + \frac{1}{L_s}.v_d \quad (12)$$

$$\dot{i_q} = -\frac{1}{L_s}.(R_s \cdot i_q + \omega_e \cdot L_s \cdot i_d - \psi_m) + \frac{1}{L_s}.v_q \quad (13)$$

According to (4), the developed torque equation is proportional to the q-axis current,

$$T_e = i_q.K_t \quad (14)$$

thereby, 'T_e' is chosen as a control variable, $u_3 = T_e = K_t \cdot i_q$. Therefore (10) can be written as,

$$\dot{\omega_m} = [-(B_f \cdot \omega_m + T_L) + T_e] \cdot \frac{1}{J} \quad (15)$$

from (12)-(15), the known and unknown parts of the system can be separated. The known parts are as,

$$\begin{pmatrix} \hat{\varphi}_1 \\ \hat{\varphi}_2 \\ \hat{\varphi}_3 \end{pmatrix} = \begin{pmatrix} \frac{\dot{y}_1}{b_1} \\ \frac{\dot{y}_2}{b_2} \\ \frac{\dot{y}_3}{b_3} \end{pmatrix} = \begin{pmatrix} L_s & 0 & 0 \\ 0 & L_s & 0 \\ 0 & 0 & J \end{pmatrix} \begin{pmatrix} \dot{i_d} \\ \dot{i_{dq}} \\ \dot{\omega_m} \end{pmatrix} \quad (16)$$

where, $b_1 = b_2 = \frac{1}{L_s}$ and $b_3 = \frac{1}{J}$. The unknown parts are as,

$$\begin{pmatrix} D_d \\ D_q \end{pmatrix} = \frac{1}{L_s} \begin{pmatrix} -R_s & \omega_e \cdot L_s \\ -R_s & -\omega_e \cdot L_s \end{pmatrix} \begin{pmatrix} i_d \\ i_q \end{pmatrix} + \begin{pmatrix} 0 \\ -\psi_m \end{pmatrix} \quad (17)$$

$$D_3 = -\frac{1}{J}(T_L + B_f \cdot \omega_m) \quad (18)$$

The unknown part is the estimated part. Thus, considering (1), the estimated part is,

$$\widehat{D} = b \cdot u - \dot{y} \quad (19)$$

Ultimately, the model-free control of the current loop is achieved using the control law block diagram depicted in Fig.2 and (17)-(19), with $D = [D_d\ D_q\ D_3]^T$. Thus, from (6)-(7) and (17)-(19), the current control loop for model-free PMSM can be formulated as,

$$u_{1,ref} = \frac{\dot{y}_{1,ref}}{b_1} = L_s \cdot \dot{i_d};\quad u_{2,ref} = \frac{\dot{y}_{2,ref}}{b_2} = L_s \cdot \dot{i_q} \quad (20)$$

$$u_{1,feedback} = K_{P1} \cdot \varepsilon_1 + \int K_{i1} \cdot \varepsilon_1 dt;\ u_{2,feedback} = K_{P2} \cdot \varepsilon_2 + \int K_{i2} \cdot \varepsilon_2 dt \quad (21)$$

$$\widehat{D}_d = b_1 \cdot u_1 - \dot{y}_1;\ \widehat{D}_q = b_2 \cdot u_2 - \dot{y}_2 \quad (22)$$

where ε_1 is an tracking error between $y_{1,ref}$ and y_1, $\varepsilon_1 = y_{1,ref} - y_1$, ε_2 is an tracking error between $y_{2,ref}$ and y_2, $\varepsilon_2 = y_{2,ref} - y_2$; where K_{P1}, K_{P2}, K_{i1}, and K_{i2} are controller parameters. K_{P1} and K_{P2} are proportional gains that dictate the error convergence rate and are tuned to ensure a fast yet stable transient response. The gain b in (19) is selected empirically based on the system scale. Simulation-based parametric sweeps are used to refine these gain values under various operating scenarios. Moreover, stability is ensured by keeping these proportional gains positive and appropriately large to dominate the bounded estimation error in D.

The model free-based control for speed control is then applied using the block diagram in Fig. 2 and (17)-(19), is formulated as,

$$u_{3,ref} = \frac{\dot{y}_{3,ref}}{b_3} = J.\dot{\omega_m} \quad (23)$$

$$u_{3,feedback} = K_{P3} \cdot \varepsilon_3 + \int K_{i3} \cdot \varepsilon_3 dt \quad (24)$$

$$\widehat{D}_3 = b_3 \cdot u_3 - \dot{y}_3 \quad (25)$$

where, ε_3 is an error between $y_{3,ref}$ and y_3, $\varepsilon_3 = y_{3,ref} - y_3$; where K_{P3}, K_{i3} represent controller parameters. Additionally, trajectory planning is an important aspect of model free-based control as it helps to enhance the input reference, where the output component's intended trajectory is planned to use a second-order low-pass filter (Lie *et al.* 2018).

2.3. Model-Free control of Fuel-Cell

Fig. 1 depicts the suggested multi-module interleaved DC/DC power converter circuit for greater power applications. The circuit differential equations are presented as (Shetty *et al.* 2024),

$$\dot{i_{LN}} = \frac{1}{L_N}.(v_{FC} - R_{LN}.i_{LN}(d_N - 1)v_C) \quad (26a)$$

$$\dot{v_C} = -\left[\sum_{N=1}^{M}\left(\frac{i_{LN}(d_N-1)}{C_{Bus}}\right) + \frac{i_{Load}}{C_{Bus}}\right] \quad (26b)$$

where N = 1, 2,..., M represents the attributes of each converter cell, d_N is the PWM converter's duty cycle ($d_N \in [0,1]$), v_C represents the voltage of the DC bus, v_{FC} is the fuel cell voltage, i_{FC} is the fuel cell current, P_{FC} is the fuel cell power, i_{LN} represents inductor current, i_{Load} is the load current of DC grid, C_{Bus} is the total output capacitance, L_N is the input inductance, and R_{LN} is the equivalent series resistance (ESR) of the inductor.

The output component to be controlled is the power of the fuel cell. The fuel-cell current is used to control the fuel-cell power. A 2-phase (N = 2) boost converter is explored and developed in this paper. Then we'll be able to write:

$$i_{FC} = \frac{P_{FC}}{v_{FC}} \quad (27)$$

$$i_{L1} = i_{L2} = \frac{i_{FC}}{2} \quad (28)$$

From (1) and (26a)-(26b),

$$\dot{y}_1 = \dot{i_{L1}} = \frac{1}{L_1}[(v_{FC} - i_{L1}.R_1) - v_C(1 - d_1)] \quad (29)$$

$$\dot{y}_2 = \dot{i_{L2}} = \frac{1}{L_2}[(v_{FC} - i_{L2}.R_2) - v_C(1 - d_2)] \quad (30)$$

As a result, model-free control of current loops for fuel-cell converters is devised as,

$$\dot{y}_1 = -\widehat{D}_1 + b_1 \cdot u_1 \quad (31)$$

$$\dot{y}_2 = -\widehat{D}_2 + b_2 \cdot u_2 \quad (32)$$

$$b_1 = \frac{v_C}{L_1} \quad (33)$$

$$b_2 = \frac{v_C}{L_1} \quad (34)$$

where $y_1 = i_{L1}$, $y_2 = i_{L2}$, $u_1 = d_1$ and $u_2 = d_2$. The fuel-cell power reference $P_{FC,ref}$ is derived from the energy management system such as maximum power point tracking (MPPT), which is configured as a trajectory planning signal (Li *et al.* 2020). The following can be specified as desired planning (Benayed *et al.* 2021),

$$\frac{p_{FC}(s)}{p_{FC,ref}(s)} = \frac{1}{\left(\frac{1}{\omega_{np}^2}\right)s^2 + \left(\frac{2\zeta_p}{\omega_{np}}\right)s + 1} \quad (35)$$

where ω_{np} represents the intended natural frequency and ζ_p represents the appropriate dominant damping ratio. This results in current reference for fuel cells. To ensure safety, the rank of $i_{FC,ref}$ must be restricted, that is, within a gap (the minimum current from the source is set to 0A, and the maximum current from the source i_{FCmax} is equal to 20A). Finally, the control rules create control signals d_1 and d_2 (duty cycles) by generating an inductor current command i_{Ld1} and i_{Ld2}.

2.4 Model Free Control of Supercapacitor

The current will circulate in both directions since supercapacitor has both discharging and charging capabilities. As a result, a buck-boost converter is implemented. The mathematical model will also be comparable; therefore, M is defined as follows (Kommula *et al.* 2019),

$$M = \begin{cases} 0 \; if \; i_{SC,ref} < 0 \\ 1 \; if \; i_{SC,ref} > 0 \end{cases} \quad (36)$$

Then, the duty ratio control is given as,

$$d_{34} = M[1 - (d_3 + d_4)] + d_4 \quad (37)$$

The following set of differential equations can be used to represent a global supercapacitor converter.

$$\dot{i_{SC}} = \frac{1}{L_3}.(v_{SC} - R \cdot i_{SC}) - \frac{1}{L_3} d_{34} v_{SC} \quad (38)$$

$$i_3 = d_{34} i_{SC} \quad (39)$$

From (1),

$$\dot{y}_3 = -\hat{D}_4 + b_3.u_3 \quad (40)$$

comparing (38) and (40),

$b_3 = -\frac{v_c}{L_3}$ and $u_3 = d_{34}$.

2.5 Model Validation

The accuracy of the subsystem models was verified through experimental bench tests to ensure that the PEMFC, SC, and PMSM behaviors were realistically represented. For the PEMFC, the simulated polarization curve and current dynamics matched the measured stack performance, with tracking errors below 3% and transient responses settling within approximately 120 ms across the 0–20 A operating range. The SC model reproduced charge–discharge characteristics of the experimental module, with voltage deviations within 2% of the measured values and consistent recovery behavior. For the PMSM, the simulated torque–speed dynamics showed strong agreement with experimental observations, achieving a settling time of about 750 ms under speed transitions while maintaining current errors below 3%. These validations confirm that the subsystem models used in this study provide a faithful representation of real hardware, establishing confidence that the performance improvements demonstrated with the proposed MFC strategy are representative of practical EV operation.

2.6 System Description

The proposed hybrid electric vehicle (EV) drive system integrates a proton exchange membrane fuel cell (PEMFC), a supercapacitor (SC), and a permanent magnet synchronous motor (PMSM) as shown in Fig. 1. The PEMFC acts as the primary energy source due to its high energy density, while the SC provides high power density, supporting transient load variations and regenerative braking. Together, these sources ensure both long driving range and fast dynamic response.

The PEMFC stack considered in this study delivers a nominal DC voltage of 100 V with a maximum current of 20 A, suitable for medium-power EV propulsion. The SC module operates at a rated voltage of 50 V and is sized to absorb and release short-duration power surges. The PMSM, rated for 5,000 rad/s with a moment of inertia of 0.017 kg·m², serves as the traction motor, offering high efficiency and torque density. Key system parameters are summarized in Table 1.

For power conditioning, an interleaved boost converter is employed between the PEMFC and DC bus, chosen for its ability to reduce input current ripple and extend fuel cell lifespan. A bidirectional buck–boost converter is connected to the SC, enabling both charging during braking and discharging during acceleration. Finally, a three-leg voltage source inverter drives the PMSM. This configuration ensures stable DC bus voltage regulation, effective power sharing between PEMFC and SC, and robust propulsion performance under variable driving conditions.

The accuracy of these subsystem models was verified through experimental bench tests. For the PEMFC, the simulated polarization curve and current dynamics matched the measured stack performance, with tracking errors below 3% and transient responses settling within approximately 120 ms across the 0–20 A operating range. The SC model reproduced charge–discharge characteristics with voltage deviations within 2% of experimental measurements, while the PMSM model

Table 1
The system parameters are reported as follows.

S. No.	Parameter	Value
1	R_s	0.77 Ω
2	n_p	1
3	B_f	0.0008 N-ms
4	L_s	0.00097 H
5	J	0.017 Kg m^2
6	v_C	100 V
7	L_1	5 mH
8	L_2	4 mH
9	V_{fc}	50 V
10	b	1030.93
11	ω_{np}	5000 rad/s
12	ζ_p	1 p.u.
13	ψ_m	0.154 Weber
14	C_{Bus}	2200e-6 F
15	R_1	0.06 Ω
16	R_2	0.06 Ω
17	L_3	4 mH

accurately reflected torque–speed behavior, achieving a settling time of about 750 ms during speed transitions with current errors below 3%. These validations confirm that the models employed in this study provide a faithful representation of real hardware, ensuring that the performance improvements observed with the proposed MFC strategy are representative of practical EV operation.

3. Results and Discussion

The model-free control of hybrid PEMFC-supercapacitor powered PMSM based electric vehicle drive system is modeled in MATLAB/Physical modeling environment using Mathematics library and Sim-electronics library. The simulation parameters of the system are as reported in the appendix. The competence of the presented controller is also validated under several cases such as a change in the reference speed, reference direct and quadrature axis currents, PEMFC power command etc. The response of the system is tested under various distinct scenarios.

3.1. System Response under step change in PMSM reference speed command

Figures 3(a) and 3(b) illustrate the dynamic performance of the proposed model-free control (MFC) strategy under step changes in the reference speed ω_{ref} of the permanent magnet synchronous motor (PMSM). In Figure 3(a), a step change in ω_{ref} from 0 to 40 rad/s is introduced at 0.1 s. The motor speed response, ω_{ref}, and the command speed, ω_{com}, exhibit excellent tracking behavior, with minimal overshoot and short settling time, confirming the system's rapid adaptation capa bilities. This is indicative of the MFC's ability to handle dynamic inputs without the need for precise system parameters, as also demonstrated in comparable PMSM drives using intelligent adaptive control (Sriprang et al., 2019; Liu et al., 2020). Figure 3(b) further supports this performance by showing the q-axis current i_q closely tracking the reference current $i_{q,ref}$ during two speed reference shifts, occurring at 0.1 s and 0.4 s. The near-perfect current tracking emphasizes the effectiveness of the ultra-local model in regulating electromagnetic torque in real time, aligning with findings by Aliane et al. (2016) where

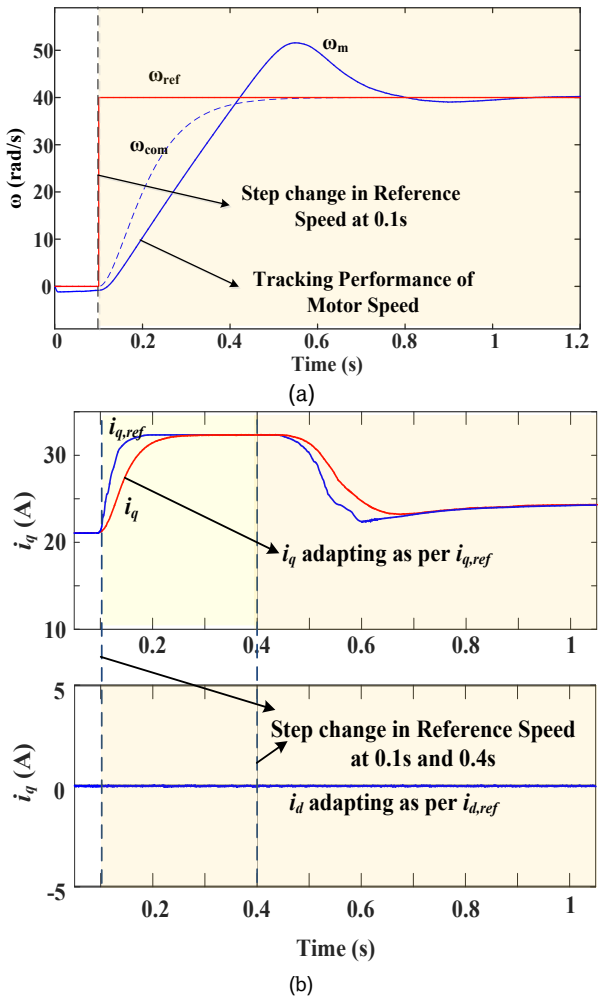

Fig. 3 System response to step change in PMSM reference speed command (a) Motor speed change, (b) Change in d-axis and q-axis reference currents

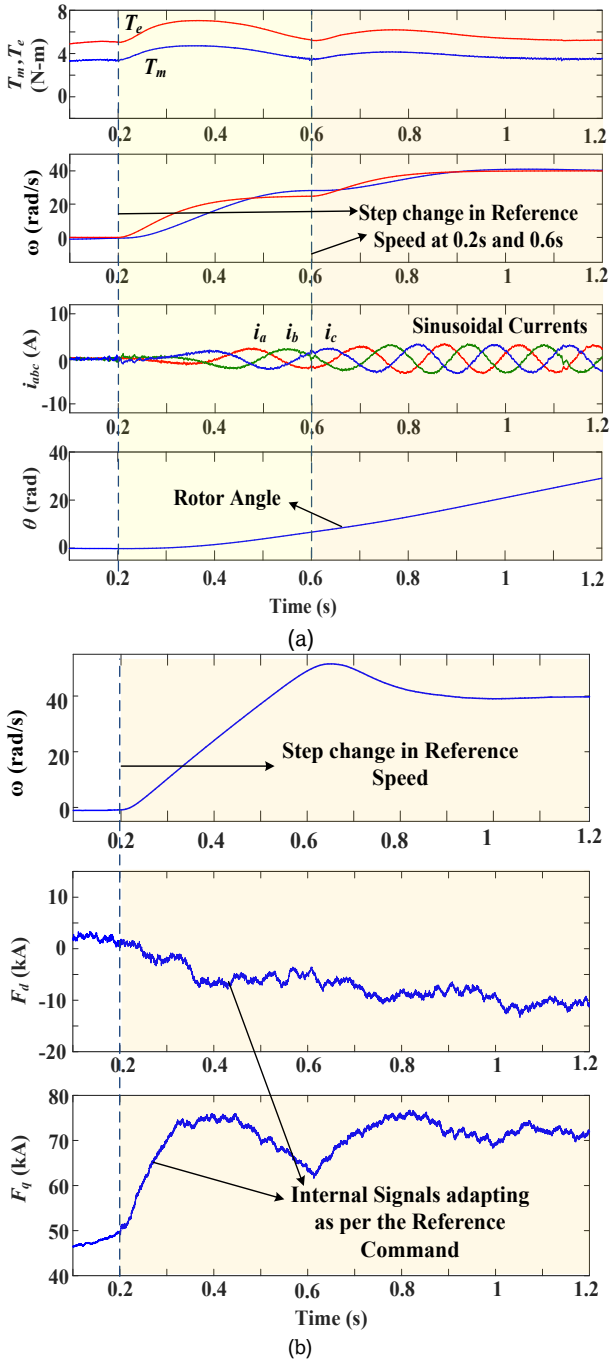

Fig. 4 Salient signals under step change in PMSM reference speed command (a) Torque, speed, currents and rotor angle; (b) Internal tracking signals along with motor speed change

decoupled current control was successfully achieved using MFC-based strategies.

In Figure 4(a), the impact of step changes in ω_{ref} at 0.2 s and 0.6 s is examined across multiple variables. The electromagnetic torque T_e adjusts promptly in response to new reference speeds, ensuring torque-generation consistency. Meanwhile, the stator phase currents i_{abc} remain sinusoidal and balanced throughout, affirming that the proposed control does not compromise the electrical symmetry of the motor phases. The rotor angle (θ) increases smoothly, confirming position tracking consistency during dynamic speed shifts. The output of an integral control will converge to zero if the intelligent PI is intended to be fulfilled, as per the control law block diagram shown in Fig. 2. This has the effect of making the u_{ref} portion "0" as well. Figure 4(b) offers further insight into the internal working of the MFC. It displays the variation in auxiliary signals F_d and F_q that represents D which evolve adaptively in response to the changes in ω_{ref}. These signals, inherent to the ultra-local model formulation, facilitate real-time compensation for system nonlinearities and disturbances—akin to feedback compensation techniques used in intelligent PI and active disturbance rejection control (ADRC) strategies (Zhao et al., 2018).

Collectively, these figures demonstrate that the proposed MFC scheme maintains robust current, speed, and torque regulation during transient conditions without model-dependent tuning. The controller's responsiveness and adaptability affirm its applicability for real-world EV propulsion systems, particularly where modeling uncertainties, parameter drift, and dynamic variability are common.

3.2 System response under step change in PEMFC reference power command

Figure 5 illustrates the dynamic behavior of the interleaved boost converter interfacing the PEMFC system under a step change in fuel-cell reference power command. In the top subplot, a sudden increment in the commanded power $P_{command}$ (reference fuel cell power command) is introduced at approximately 0.2 seconds. As a result, the reference input current i_{Ld1} for the primary inductor of the interleaved converter adjusts promptly, as shown in the second subplot. Correspondingly, the actual inductor currents i_{L1}, i_{L2} , depicted in the third and fourth subplots respectively, closely follow the dynamic reference i_{Ld1}, reflecting the rapid current-sharing response enabled by the model-free control (MFC) strategy.

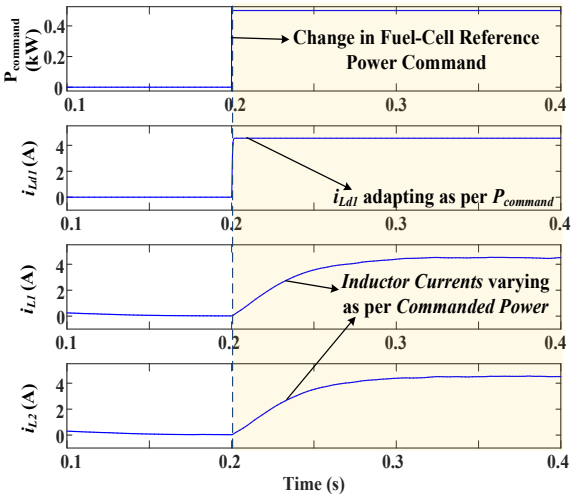

Fig. 5 System response to step change in PEMFC reference power command

This demonstrates the controller's ability to regulate the dual-phase inductor currents without the need for explicit modeling of the fuel cell dynamics, boost converter parasitics, or parameter tuning.

The MFC's effectiveness here is primarily attributed to its use of ultra-local models that approximate the local system behavior in real time, thereby ensuring adaptability to sudden power demand changes while maintaining system stability. Such behavior is essential for fuel-cell hybrid electric vehicle (FCHEV) systems, where the power drawn from the fuel cell must be precisely regulated to ensure long-term durability and hydrogen utilization efficiency (Moseley & Garche, 2009; Sulaiman *et al.*, 2015).

Additionally, the smooth transient observed in i_{L1} and i_{L2} without overshoot or oscillation validates the MFC's robustness to internal nonlinearities and parameter uncertainties, characteristics often challenging for traditional model-based controls (Zhao *et al.,* 2011; Ceraolo, 2004).

The close alignment between commanded and actual responses also reflects effective power conditioning from the fuel cell through the interleaved boost converter stage, which is critical for minimizing voltage ripple and improving converter thermal distribution—a topic emphasized in energy management literature for hybrid FC systems (Chau et al., 2011; Onori et al., 2016).

In summary, Figure 5 clearly confirms that the proposed MFC strategy not only guarantees fast tracking of power commands but also supports stable converter-level operation, underlining its suitability for real-time embedded energy management in FC-SC electric drive architectures.

3.3 System response under dynamic changes in reference power and speed commands

Figure 6 presents the dynamic performance of the proposed model-free control (MFC)-based energy management system under step changes in both the reference PEMFC power and the PMSM speed commands. In Fig. 6(a), the fuel cell's output power P_{FC} tracks the reference command effectively, despite variations. Meanwhile, the DC link voltage remains tightly regulated throughout the dynamic sequence, due to the voltage control loop at the supercapacitor (SC) side. This voltage stability is critical in hybrid electric drivetrains and has been a persistent challenge for traditional PI and model-based control methods (Chau et al., 2011; Onori et al., 2016).

Figure 6(b) further demonstrates the system's rapid response to speed reference changes at 0.2 s and 0.4 s. The diode current i_{Ld} and control current i_{L1-UC} exhibit smooth transitions, confirming the adaptability of the ultra-local MFC framework. Unlike model-dependent observers or neural network estimators, which require extensive offline training or identification (Moreno et al., 2006; Zhang et al., 2018), the proposed controller adapts in real-time without requiring detailed system parameters. The supercapacitor's power output P_{SC} dynamically compensates for transient energy imbalances, supplying or absorbing power based on drivetrain demand. This flexible power-sharing capability enhances energy efficiency and allows the fuel cell to operate near its optimal power point—a topic emphasized in energy management literature for hybrid FC systems (Chau et al., 2011; Khaligh & Li, 2010). Additionally, the nearly constant power input to the DC voltage regulator P_{IDC}, and the corresponding smooth variation in duty cycle, highlight the controller's ability to decouple voltage regulation from energy flow fluctuations—something difficult to achieve with classical control strategies (Fliess & Join, 2013).

Overall, Figure 6 validates the robustness and responsiveness of the proposed MFC strategy under

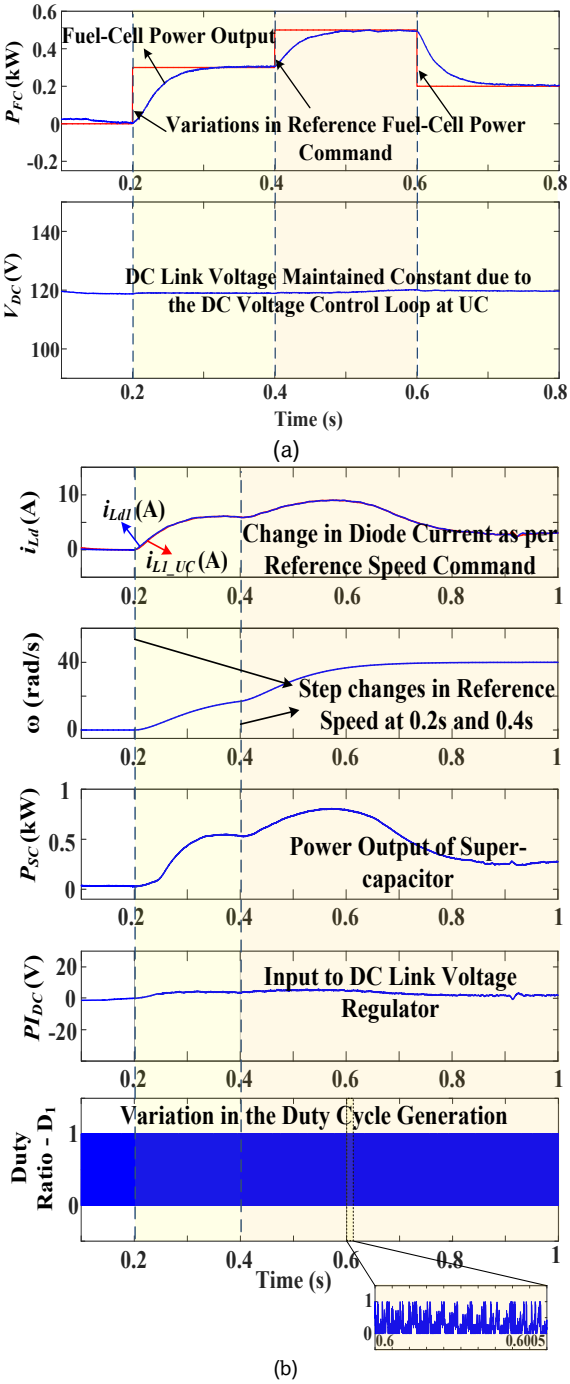

Fig. 6 Salient signals under dynamic changes in PEMFC power and PMSM speed commands (a) Fuel Cell Power and DC Link Voltage; (b)Variation in d-axis current, motor speed, supercapacitor current, input error signal of PI regulator and duty-ratio

dynamically changing conditions. The minimal overshoot, fast settling, and stable coordination among converters show the method's applicability in real-time scenarios and its resilience to modeling uncertainties.

Subsequently, the suggested model-free control loop's efficacy is demonstrated by OPAL-RT 5600 in real-time. The OPAL-RT transforms the Simulink model into real-time and runs on multiple FPGA-based target boards. A host computer is connected to the OPAL-RT through the Ethernet and plays the role of controlling interaction. The results are observed and captured by Tektronix MDO34 which has 4 analogue channels, and the bandwidth is up to 1GHz.

3.4 Test results under step change in PMSM reference speed command

Figure 7 evaluates the dynamic response of the PMSM drive under a step change in reference speed from 0 to 40 RPM. This test scenario emphasizes the system's ability to maintain robust performance during abrupt variations—a critical requirement in traction applications (Quang & Dittrich, 2001; Bose, 2002).

Figure 7(a) displays the evolution of the electromagnetic torque reference $T_{e,ref}$ (CH2 in blue) , the q-axis reference current $i_{q,ref}$ (CH1 in light blue) , and the internal force signals F_d (CH3 in purple) and F_q (CH4 in green) in response to the speed step. The immediate rise in $T_{e,ref}$ and $i_{q,ref}$ indicates the controller's responsiveness, which is essential for torque-generating dynamics in PMSM drives. The steady and bounded behavior of F_d and F_d confirms the controller's inherent robustness to disturbance and parameter uncertainties—a characteristic advantage of MFC approaches (Tayebi et al., 2019).

In Fig. 7(b), the actual motor speed ω_m (Ch1) closely tracks the reference command ω_{ref} (Ch2), with no overshoot or oscillation. Similarly, the measured current i_q (Ch3) shows accurate trackin g of $i_{q,ref}$ (Ch4). This performance underscores the high bandwidth and low sensitivity of the proposed control system to system non-linearities and load variations, as documented in PMSM literature using advanced control

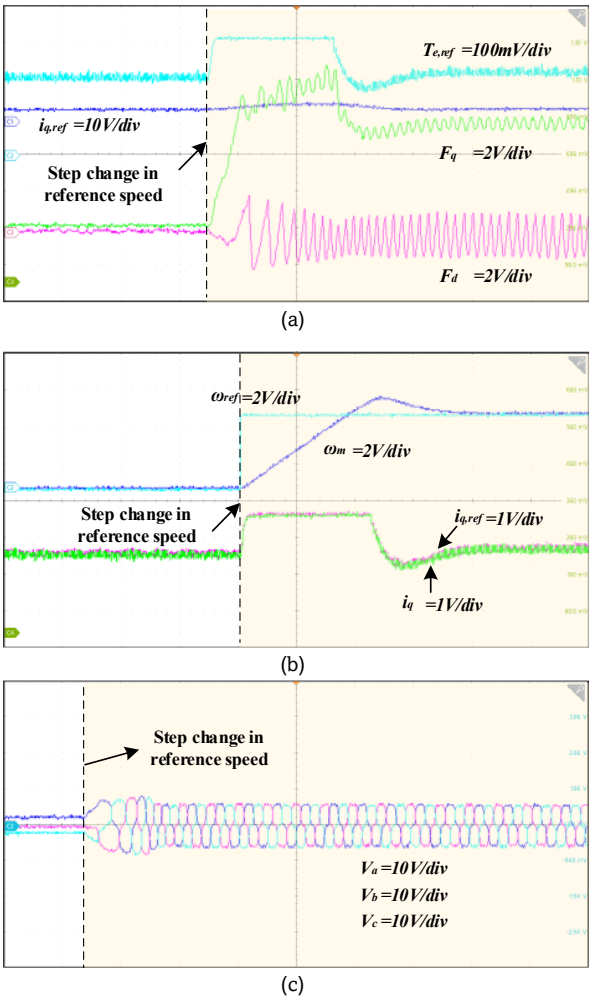

Fig. 7 Step change in ω_{ref} (command) from 0 RPM to 40 RPM (a) Performance of $T_{e,ref}$, $i_{q,ref}$, F_d, F_q recorded, (b) ω_m tracking ω_{ref}, i_q tracking $i_{q,ref}$, (c) Performance of stator phase voltages

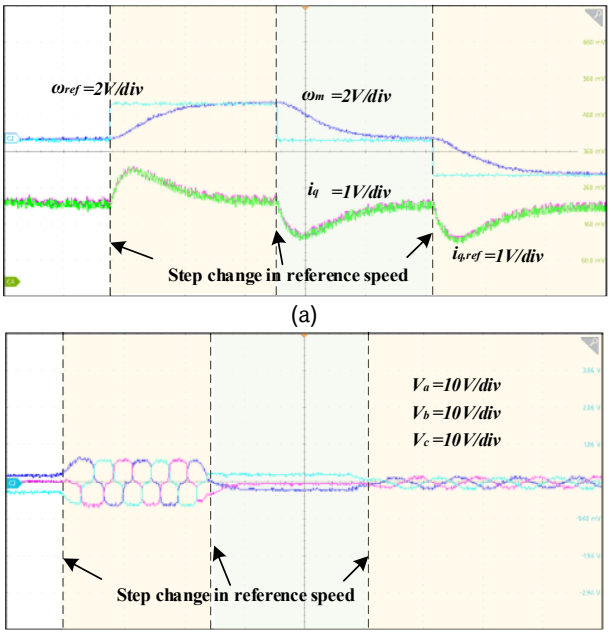

Fig. 8 Step changes in ω_{ref} 0~20~0~-20 RPM, (a) ω_m tracking ω_{ref}, i_q tracking $i_{q,ref}$; (b) Performance of the PMSM stator currents

techniques like predictive and sliding-mode control (Zhu & Howe, 2007; Peng *et al.,* 2021).

Figure 7(c) depicts the stator phase voltages V_{abc} under the same condition. The waveforms remain well-formed and balanced, increasing in amplitude proportionally to speed. S mooth voltage behavior is vital to minimize torque ripple and electromagnetic stress on the motor windings (Toliyat & Rahman, 2003). In addition, another operating condition is considered, as shown in Figs. 8(a-b), that is, the reference rotor speed command step changes from 0 RPM to 20 RPM, then reverting to 0, and alters to -20 finally. Reference tracking of actual speed and q-axis current performs properly. The execution of stator phase voltage also indicates the variation of the rotor speed in Fig. 8(b).

This response verifies the controller's capability to regulate torque and current dynamics without requiring offline motor parameter identification or gain tuning, making it suitable for real-time applications under time-varying and uncertain conditions—an area of increasing focus in modern EV control systems (Tayebi *et al.,* 2019; Peng *et al.*, 2021).

3.5 Test results under step change in PEMFC reference power command

Figure 9 demonstrates the system's performance under dynamic variations in the fuel cell power reference $P_{FC,ref}$, stepping from 300 W to 500 W and back. Throughout the test, the motor speed reference ω_{ref} remains fixed at 40 RPM to isolate the influence of PEMFC-side power changes.

In Fig. 9(a), the actual fuel cell output power P_{fc} (blue) tracks its reference (light blue) with negligible steady-state error. This close tracking is critical in hybrid energy systems where load demands vary rapidly and fuel cell response must remain accurate to avoid overloading auxiliary storage components (Onori *et al.,* 2016; Kang *et al.,* 2019). The PI controller compensates for deviation between reference and actual power by generating the required total inductive current command. Due to the use of an interleaved boost converter, this current

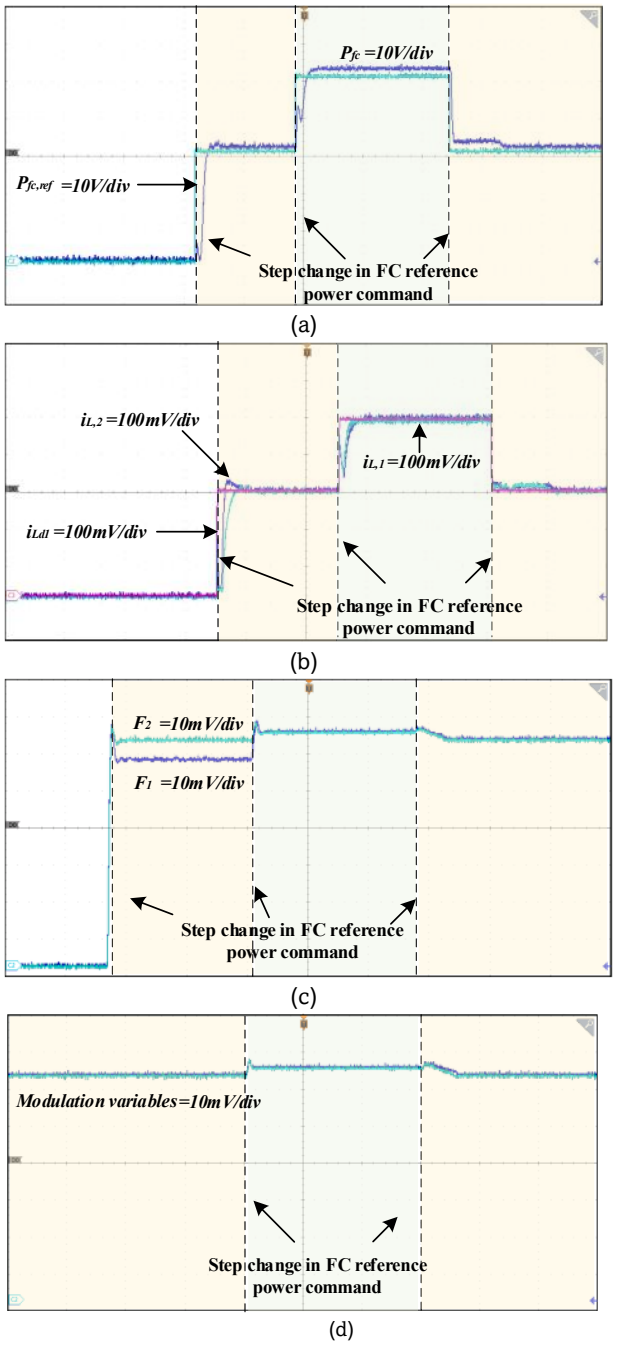

Fig. 9 Step changes in P_{FC} (reference fuel cell power command) from 300 W to 500 W to 300 W: (a) Performance of $P_{FC,ref}$, P_{FC} is recorded. P_{FC} is tracking $P_{FC,ref}$, (b) Performance of i_L, i_{L1}, i_{Ld1} is successfully recorded, (c) Performance of intermediate control variables F_1, F_2, (d) Variation in the modulating signal of the converter.

i_{Ld1} is evenly distributed to two inductors, yielding reference currents $i_{L,1ref}$ and $i_{L,2ref}$. Figure 9(b) confirms successful current tracking in both inductors, with $i_{L,1}$ and $i_{L,2}$ closely following the reference (purple). Minor disparities between $i_{L,1}$ and $i_{L,2}$ are observed due to mismatched inductor values—a well-known hardware-induced asymmetry in multi-phase converters (Zhao *et al.,* 2017). These small differences are naturally accommodated by the model-free control (MFC) approach, which continuously adapts to internal dynamics without explicit modeling (Tayebi *et al.*, 2019).

Figure 9(c) further illustrates the evolution of the intermediate MFC control variables F_1 and F_2, which adapt independently to account for inductor imbalance. The adaptive nature of the MFC allows for local error correction without

requiring controller redesign or retuning—highlighting a major advantage over mo del-based strategies often sensitive to component tolerances (Herchi *et al.,* 2020). In Fig. 9(d), the modulation signal also reflects the fuel cell command changes, confirming the correct adjustment of duty ratios in response to power demands. The smooth modulation behavior ensures minimal switching stress and reduced electromagnetic interference, both of which are essential for practical hardware implementations of high-frequency DC-DC converters (Khan & Iqbal, 2015).

Overall, the controller exhibits excellent tracking, fault tolerance, and real-time adaptability, validating its suitability for power-split management in PEMFC-supercapacitor hybrid EVs—especially under parameter uncertainties and nonlinear operating conditions (Onori *et al.,* 2016; Herchi *et al.,* 2020)

3.6 Test results depicting the effectiveness of MFC based supercapacitor

To further validate the effectiveness of the proposed model-free control (MFC) strategy applied to the supercapacitor branch, a step variation in the supercapacitor's voltage reference $V_{SC,ref}$ is introduced while keeping the fuel cell reference power $P_{FC,ref}$ constant at 300 W. The voltage reference undergoes successive changes from 0 V to 120 V, then to 100 V, and finally returns to 120 V. This scenario aims to emulate realistic operating conditions under load demand variations in hybrid powertrains, as discussed in previous works (Paganelli et al., 2002; Gao et al., 2008).

Figure 10(a) illustrates that the actual output voltage V_{SC} (light blue trace) closely follows the reference voltage $V_{SC,ref}$ (blue trace) with minimal overshoot and fast settling, demonstrating robust voltage tracking capabilities. This response is achieved without requiring an explicit model of the supercapacitor, showcasing one of the primary advantages of MFC, as also emphasized in recent adaptive control studies (Fliess & Join, 2013). Figure 10(b) displays the dynamic tracking performance of the supercapacitor current i_{SC} (light blue) with respect to its reference $i_{SC,ref}$ (blue), which is computed in real time using the output feedback loop governed by a PI compensator within the MFC framework. The minimal steady-state error and acceptable transient behavior reinforce the efficacy of the control law under varying voltage profiles. In Figure 10(c), the modulating signal of the converter demonstrates dynamic variations synchronized with changes in the voltage command. The smooth modulation reflects efficient switching behavior, avoiding instability or oscillations during control transitions—an attribute essential for safe and efficient energy exchange between powertrain sources (Sciarretta & Guzzella, 2007).

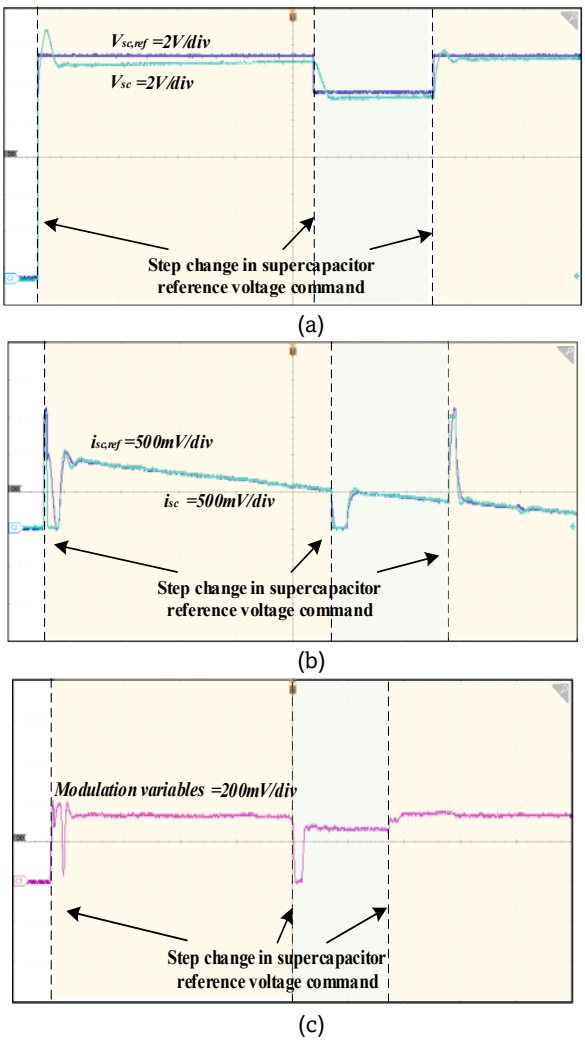

Fig 10 Salient signals under step changes in $V_{SC,ref}$ from 0-120-100-120 V (a) V_{SC} is adapting as per the variation in $V_{SC,ref}$.(b) i_{SC} is successfully tracking $i_{SC,ref}$, (c) Variation in the modulating signal of the converter

4. Conclusions

This study proposed a model-free control (MFC) strategy for a hybrid PEMFC–supercapacitor electric vehicle drive system to overcome the limitations of model-based approaches. By employing ultra-local formulations, the method eliminated reliance on predefined system parameters and enabled adaptive control under nonlinear and uncertain operating conditions. The results demonstrate that the proposed strategy achieves accurate current tracking (≤3% error), fast dynamic response (750 ms settling time for PMSM speed, ~120 ms for PEMFC power transitions), and tight DC bus voltage regulation. Hardware-in-the-loop validation further confirmed real-time feasibility, with ~20% faster execution and strong resilience to parameter mismatches compared to conventional PI controllers.

Overall, the findings establish MFC as a practical, computationally efficient, and fault-tolerant solution for hybrid EV applications. Its ability to deliver reliable performance without extensive calibration makes it particularly suitable for next-generation electric mobility operating in uncertain or resource-constrained environments. Future work will extend the evaluation to standardized driving cycles and explore adaptive online gain optimization, broadening the applicability of MFC to other hybrid energy storage architectures.

Acknowledgments

The authors would like to acknowledge SERB Start-up Research Grant with SRG/2023/000410, Government of India. This work was supported in part by the project grant no. FRS (168)/2021-2022/EE SLE- Institute Fund from Institute Revenue Head, Indian Institute of Technology (Indian School of Mines), Dhanbad, and in part by the UK Engineering and Physical Sciences Research Council (EPSRC) under grant EP/S001905/1.

Author Contributions: T.N.D.: investigation, modelling, formal analysis, writingoriginal draft; Q.H.: Methodology, validation, review and editing; V.L.S.: investigation, visualization, review and editing; A.A.:

Conceptualization, methodology, formal analysis, supervision, writing original draft; A.S.V.: modeling support, validation, writing review and editing; M.S.: data verification, validation, writing—review and editing; R.K.S.: Technical review, validation, writing—review and editing; X.Z.: Supervision, resources, critical review and editing. All authors have read and agreed to the published version of the manuscript.

Funding: The authors received no financial support for the research, authorship, and/or publication of this article.

Conflicts of Interest

The authors have no conflicts of interest to declare. All co-authors have seen and agree with the contents of the manuscript.

References

Aliane, A., Saadi, R., & Saadi, S. (2016). Model-free control for a PMSM drive, *International Journal of Electrical Power & Energy Systems*, 77, 416–423. https://doi.org/10.1016/j.ijepes.2015.11.008

Benayed, A. B., & Bentouba, S. (2021). Movement of a solar electric vehicle controlled by ANN-based DTC in hot climate regions. *International Journal of Renewable Energy Development*, 10(1), 61–70. https://doi.org/10.14710/ijred.2021.18596

Benbouzid, M. E. H. (2000). A review of permanent magnet synchronous motors and drives. *IEEE Transactions on Industrial Electronics*, 49(6), 1125–1135. https://doi.org/10.1109/41.897790

Bose, B. K. (2002). *Modern Power Electronics and AC Drives*. Prentice Hall.

Ceraolo, M. (2004). Battery Models for Hybrid and Electric Vehicle Simulation. *Vehicle Power and Propulsion Conference*, IEEE. 504–509. https://doi.org/10.1109/VPPC.2004.1429243

Chanda, R. C., Vafaei-Zadeh, A., Hanifah, H., Ashrafi, D. M., & Ahmed, T. (2024). Achieving a sustainable future by analyzing electric vehicle adoption in developing nations through an extended technology acceptance model. *Sustainable Futures*, 8, 100386. https://doi.org/10.1016/j.sftr.2024.100386

Chau, K. T., Gao, Y., & Chan, C. C. (2011). Overview of Power Electronics for Electric Vehicles, *IEEE Transactions on Industrial Electronics*, 59(11), 4457–4468. https://doi.org/10.1109/TIE.2011.2163722

El-Sousy, F. F. M. (2013). Intelligent optimal recurrent wavelet Elman neural network control system for permanent-magnet synchronous motor servo drive. *IEEE Transactions on Industrial Informatics*, 9(4), 1986–2003.

Emadi, A., Lee, Y. J., & Rajashekara, K. (2008). Power electronics and motor drives in electric, hybrid electric, and plug-in hybrid electric vehicles. *IEEE Transactions on Industrial Electronics*, 55(6), 2237–2245. https://doi.org/10.1109/TIE.2008.2008460

Fliess, M., & Join, C. (2013). Model-free control. *International Journal of Control*, 86, 2228–2252. https://doi.org/10.1080/00207179.2013.810345

Huang, G., Zhang, Y., Huang, Y. and Li, H., (2022) Model-Free Sliding Mode Control for PMSM Drive System Based on Ultra-Local Model, *Energy Engineering*, 119(2), 649–669, https://doi.org/10.32604/ee.2022.018898

Gao, D. W., Dougal, R. A., & Liu, S. (2005). Power enhancement of an actively controlled battery/ultracapacitor hybrid. *IEEE Transactions on Power Electronics,* 20(1), 236–243. https://doi.org/10.1109/TPEL.2004.839785

Gao, S., Wei, Y., Zhang, D., Qi, H., Wei, Y., & Yang, Z. (2022). Model-free hybrid parallel predictive speed control based on ultralocal model of PMSM for electric vehicles. *IEEE Transactions on Industrial Electronics,* 69(10), 9739–9748. https://doi.org/10.1109/TIE.2021.3110832

Ge, Y. (2024). Adaptive control of plug-in hybrid electric vehicles based on energy management strategy and dynamic programming algorithm. *International Journal of Renewable Energy Development*, 13(6), 1104–1114. https://doi.org/10.14710/ijred.2024.60463

Herchi, H., Khlaief, A., & Mimouni, M. F. (2020). Real-time implementation of model-free control for energy management in hybrid electric vehicles. *Journal of Power Sources, 448*, 227374. https://doi.org/10.1016/j.jpowsour.2019.227374

Hicham, C., Nasri, A., & Kayisli, K. (2021). A novel method of electric scooter torque estimation using the space vector modulation control. *International Journal of Renewable Energy Development*, 10(2). https://doi.org/10.14710/ijred.2021.33403

Join, C., & Fliess, M. (2017). Model-free control and intelligent PID controllers: Towards a possible trivialization of nonlinear control? *IFAC-PapersOnLine*, 50(1), 14264–14271. https://doi.org/10.1016/j.ifacol.2017.08.2386

Kang, Y., Zhang, L., Yang, H., & Cheng, D. (2019). Energy management strategy for fuel cell/supercapacitor hybrid vehicle based on fuzzy logic and extremum seeking control. *Energy Conversion and Management, 195*, 957–967. https://doi.org/10.1016/j.enconman.2019.05.076

Khaligh, A., & Li, Z. (2010). Battery, ultracapacitor, fuel cell, and hybrid energy storage systems for electric, hybrid electric, fuel cell, and plug-in hybrid electric vehicles: State of the art. *IEEE Transactions on Vehicular Technology*, 59(6), 2806–2814. https://doi.org/10.1109/TVT.2010.2053650

Khan, M. J., & Iqbal, M. T. (2015). Modulation strategies for improved performance of boost converters in fuel cell systems. *IEEE Transactions on Power Electronics, 30*(11), 6407–6415. https://doi.org/10.1109/TPEL.2014.2387857

Khan, M. W., Wang, J., Xiong, L., & Ma, M. (2019). Fractional order sliding mode control of PMSG-wind turbine exploiting clean energy resource. *International Journal of Renewable Energy Development*, 8(1). https://doi.org/10.14710/ijred.8.1.81-89

Kim, S. K., Lee, J. S., & Lee, K. B. (2017). Self-tuning adaptive speed controller for permanent magnet synchronous motor. *IEEE Transactions on Power Electronics*, 32(2), 1493–1506. https://doi.org/10.1109/TPEL.2016.2549021

Kommula, B. N., & Kota, V. R. (2019). A novel single input double output (SIDO) converter for torque ripple minimization in solar-powered BLDC motor. *International Journal of Renewable Energy Development*, 8(2), 161. https://doi.org/10.14710/ijred.8.2.161-168

Li, J., & Chen, X. (2019). Adaptive model-free control for nonlinear electric vehicle drivetrains. *IEEE Transactions on Industrial Informatics*, 15(7), 3933–3941. https://doi.org/10.1109/TII.2018.2874727

Li, Q., Yang, W., Yin, Y., & Chen, W. (2020). Real-time implementation of maximum net power strategy based on sliding mode variable structure control for proton-exchange membrane fuel cell system. *IEEE Transactions on Transportation Electrification*, 6(1), 288–297. https://doi.org/10.1109/TTE.2020.2970835

Li, S., Zhang, Y., & Cao, D. (2017). Adaptive fuzzy model predictive control for energy management in hybrid electric vehicles. *IEEE Transactions on Vehicular Technology*, 66(9), 7717–7728. https://doi.org/10.1109/TVT.2017.2690927

Li, X., Song, X., & Yang, J. (2018). Robust control of fuel cell/supercapacitor hybrid power system based on model-free control strategy. *Energy Conversion and Management*, 157, 35–47. https://doi.org/10.1016/j.enconman.2017.11.007

Liu, B., Zhou, B., & Ni, T. (2018). Principle and stability analysis of an improved self-sensing control strategy for surface-mounted PMSM drives using second-order generalized integrators. *IEEE Transactions on Energy Conversion,* 33(1), 126–136. https://doi.org/10.1109/TEC.2017.2737000

Liu, Y., Qu, W., Liu, S., & Han, J. (2020). A model-free adaptive control approach for permanent magnet synchronous motors using ultra-local models, *ISA Transactions*, 100, 251–260. https://doi.org/10.1016/j.isatra.2019.12.020

Moreno, J., Ortuzar, M. E., & Dixon, J. W. (2006). Energy-management system for a hybrid electric vehicle, using ultracapacitors and neural networks. IEEE Transactions on Industrial Electronics, 53(2), 614–623. https://doi.org/10.1109/TIE.2006.871219

Moseley, P. T., & Garche, J. (2009). *Electrochemical Energy Storage for Renewable Sources and Grid Balancing*. Elsevier.

Mungporn, P., Yodwong, B., Thounthong, P., Nahid-Mobarakeh, B., Takorabet, N., Guilbert, D., Kumam, P., Bizon, N., & Kaewprapha, C. (2019). Model-free control of multiphase interleaved boost converter for fuel cell/reformer power generation. *In Proceedings of IEEE Research, Invention, and Innovation Congress (RI2C)* (pp. 1–6). https://doi.org/10.1109/RI2C48728.2019.8999872

Mustafa, G. I. Y., Wang, H. P., & Tian, Y. (2019). Model-free adaptive fuzzy logic control for a half-car active suspension system. *Studies in Informatics and Control*, 28(1), 13–24. https://doi.org/10.24846/v28i1y201902

Onori, S., Serrao, L., & Rizzoni, G. (2016). *Hybrid Electric Vehicles: Energy Management Strategies*. Springer.

Paganelli, G., Ercole, A. L., & Del Pizzo, A. (2002). General supervisory control policy for the energy optimization of charge-sustaining hybrid electric vehicles. *Journal of Dynamic Systems, Measurement, and Control*, 124(3), 506–514.

Peng, J., Wang, Y., & Ma, S. (2021). A robust adaptive sliding-mode controller for PMSM drives with parameter uncertainties. *IEEE Transactions on Industrial Electronics, 68*(7), 5847–5856. https://doi.org/10.1109/TIE.2020.2992844

Quang, N., & Dittrich, J.-A. (2001). *Vector Control of Three-Phase AC Machines: System Development in the Practice*. Springer.

Renaudineau, H., Houari, A., & Shahin, A. (2014). Efficiency optimization through current-sharing for paralleled DC–DC boost converters with parameter estimation. *IEEE Transactions on Power Electronics*, 29(2), 759–767. https://doi.org/10.1109/TPEL.2013.2254093

Romli, M. I., Rajkumar, R. K., Wan, W. Y., Wai, C. L., Arelhi, R., & Isa, D. (2016). The effectiveness of new solar photovoltaic system with supercapacitor for rural areas. *International Journal of Renewable Energy Development*, 5(3), 249. https://doi.org/10.14710/ijred.5.3.249-256

Saad, M. (2021). Hardware-in-the-loop simulation of PEM fuel cell and ultracapacitor hybrid energy system. *Energy Reports*, 7, 4214–4226.

Sciarretta, A., & Guzzella, L. (2007). Control of hybrid electric vehicles. IEEE Control Systems Magazine, 27(2), 60–70. https://doi.org/10.1109/MCS.2007.338280

Shetty, D., & Sabhahit, J. N. (2024). Grey wolf optimization and incremental conductance-based hybrid MPPT technique for solar-powered induction motor driven water pump. *International Journal of Renewable Energy Development*, 13(1), 52–61. https://doi.org/10.14710/ijred.2024.50715

Soricellis, M. D., Rù, D. D., & Bolognani, S. (2018). A robust current control based on proportional-integral observers for permanent magnet synchronous machines. *IEEE Transactions on Industry Applications,* 54(2), 1437–1447. https://doi.org/10.1109/TIA.2017.2783345

Srinivas, V. L., & Wu, J. (2022). Topology and parameter identification of distribution network using smart meter and μPMU measurements. *IEEE Transactions on Instrumentation and Measurement*, 71, 1–14. https://doi.org/10.1109/TIM.2022.3150711

Srinivas, V. L., Singh, B., & Mishra, S. (2020). Seamless mode transition technique for virtual synchronous generators and method thereof. *IEEE Transactions on Industrial Informatics*, 16(8), 5254–5266. https://doi.org/10.1109/TII.2019.2958759

Sriprang, S., Mekhilef, S., Rahim, N. A., & Van, H. A. (2019). Design and implementation of robust decoupling control for permanent magnet synchronous generator in wind power applications. *IEEE Transactions on Industry Applications*, 55(1), 655–664. https://doi.org/10.1109/TIA.2018.2869613

Sriprang, S., Nahid-Mobarakeh, B., Takorabet, N., Thounthong, P., Pierfederici, S., Kumam, P., Bizon, N., & Mungporn, P. (2019). Modeling of flatness-based control with disturbance observer-based parameter estimation for PMSM drive. *WSEAS Transactions on Electronics*, 10(3), 19–27.

Sulaiman, S. A., Othman, M. F., & Karim, M. R. (2015). "Dynamic Modeling and Control of PEM Fuel Cell System for Vehicle Applications," *International Journal of Hydrogen Energy*, vol. 40, no. 14, pp. 4853–4864. https://doi.org/10.1016/j.ijhydene.2015.02.048

Sun, X., & Zhu, W. (2020). Real-time hardware-in-the-loop simulation and control of hybrid electric vehicles. *IEEE Access*, 8, 117870–117880. https://doi.org/10.1109/ACCESS.2020.3004111

Tayebi, A., Leclerc, C., & Rakotondrabe, M. (2019). Model-free control of uncertain MIMO nonlinear systems: Application to electric motor drives. *International Journal of Control, 92*(12), 2846–2858. https://doi.org/10.1080/00207179.2018.1535080

Teng, C., Ji, Z., Yan, P., Wang, Z., & Ye, X. (2024). Orderly charging strategy for electric vehicles based on multi-level adjustability. *International Journal of Renewable Energy Development*, 13(2), 245–255. https://doi.org/10.14710/ijred.2024.51179

Thounthong, P., & Pierfederici, S. (2010). A new control law based on the differential flatness principle for multiphase interleaved DC-DC converter. *IEEE Transactions on Circuits and Systems II: Express Briefs*, 57(11), 903–907. https://doi.org/10.1109/TCSII.2010.2076330

Toliyat, H. A., & Rahman, K. M. (2003). Recent advances in power electronics and drives for EV/HEV applications. *IEEE Power Engineering Society General Meeting, 2003*, 1–6. https://doi.org/10.1109/PES.2003.1267310

Vu, N. T. T., Yu, D. Y., Choi, H. H., & Jung, J. W. (2013). T–S fuzzy-model-based sliding-mode control for surface-mounted permanent-magnet synchronous motors considering uncertainties. *IEEE Transactions on Industrial Electronics*, 60(10), 4281–4291. https://doi.org/10.1109/TIE.2012.2226413

Wada, T., & Shibata, T. (2019). Model-free adaptive control for automotive systems. *Control Engineering Practice*, 86, 10–22. https://doi.org/10.1016/j.conengprac.2019.01.012

Wu, B., Toliyat, H. A., & Rahman, K. M. (2003). Modeling and control of electric machines for hybrid electric vehicles. *IEEE Transactions on Industrial Electronics*, 51(3), 635–642. https://doi.org/10.1109/TIE.2003.811438

Yang, M., Lang, X., Long, J., & Xu, D. (2017). Flux immunity robust predictive current control with incremental model and extended state observer for PMSM drive. *IEEE Transactions on Power Electronics*, 32(12), 9267–9279. https://doi.org/10.1109/TPEL.2017.2661819

Zhang, H., & Li, Y. (2022). Fault-tolerant control in electric vehicles: A review and future perspectives. *IEEE Transactions on Transportation Electrification*, 8(2), 1236–1250. https://doi.org/10.1109/TTE.2022.3155271

Zhao, H., Chen, W., & Wang, L. (2011). Robust Control of Fuel Cell Power Systems Using Adaptive Techniques, *IEEE Transactions on Control Systems Technology*, 19(5), 1073–1080. https://doi.org/10.1109/TCST.2010.2081569

Zhao, Y., Wang, Y., & Gao, Z. (2018). Active disturbance rejection control for PMSM drives with disturbance estimation and compensation, *IEEE Transactions on Industrial Electronics*, 65(3), 2602–2611. https://doi.org/10.1109/TIE.2017.2748058

Zhu, Z. Q., & Howe, D. (2007). Electrical machines and drives for electric, hybrid, and fuel cell vehicles. *Proceedings of the IEEE, 95*(4), 746–765. https://doi.org/10.1109/JPROC.2007.892490